Theoretical analysis and computer simulation of fluorescence lifetime measurements. II. Contour length dependence of single polymers

Shilong Yang and Jianshu Cao[a)]
Department of Chemistry, Massachusetts Institute of Technology, Cambridge, Massachusetts 02139

(Received 9 March 2004; accepted 6 April 2004)

Fluorescence lifetime measurements in a polymer chain are modeled using a memory function expansion, computer simulations, and simple scaling arguments. Unless the quenching rate is localized and infinitely fast, the fluorescence lifetime is generally not equivalent to the first passage time. The fluorescence lifetime distribution is decomposed into memory functions that can be measured separately in single-molecule experiments. The leading order of the expansion gives the Wilemski–Fixman (WF) approximation, and the convergence of higher order terms determines its validity. Simulations of the fluorescence quenching on a Rouse chain verify the accuracy of the WF approximation at small contact radii, short contour lengths, and small quenching rates. Detailed investigation of the average fluorescence lifetime reveals two competing mechanisms: the independent motion of end-to-end vector, which dominates at small contact radius, and the slowest relaxation of polymer, which dominates at large contact radius. The Wilemski–Fixman rate is used in combination with scaling arguments to predict the dependence of fluorescence lifetime on the contour length. Our predictions for the scaling of the average lifetime with the contour length are in good agreement with both simulations and recent experiments by Eaton and his group [L. J. Lapidus, W. A. Eaton, and J. Hofrichter, Proc. Natl. Acad. Sci. U.S.A. **97**, 7220 (2000)]. © *2004 American Institute of Physics.* [DOI: 10.1063/1.1756578]

I. INTRODUCTION

Fluorescence quenching on a polymer chain has been of theoretical and experimental interest for a long time.[1–4] The strong dependence of quenching rate on the fluorophore-quencher distance makes fluorescence quenching a sensitive probe of the loop formation dynamics in polypeptides and DNAs. Recent developments in time-resolved single-molecule fluorescence spectroscopy provide new tools to understand conformational dynamics on the molecular level.[5–9] The internal relaxation of the polymer makes the quenching reaction a complicated example of diffusion-controlled reactions. Over several decades, there have been extensive discussions of diffusion-controlled reactions.[10–18] A widely used approximation scheme to calculate intra-chain reactions in dilute solutions was first presented by Wilemski and Fixman,[10,11] which is referred to here as the WF approximation. The main focus of this paper is to quantify the reliability of the WF approximation for a Gaussian chain, validate the criteria with computer simulations, and predict the contour length dependence of the average fluorescence lifetime.

In paper I of this series, we studied two different regimes of the reaction kinetics modulated by conformational fluctuations and accounted for the effects of the experimental observation window in fluorescence measurements.[19] The stationary reaction process dominates in the configuration-controlled regime while the diffusion process dominates in the diffusion-controlled regime. A path integral simulation was used to model fluorescence quenching processes on a semiflexible chain. We demonstrated that the first-order inhomogeneous cumulant expansion in the configuration-controlled regime defines a lower bound for the survival probability, while the WF approximation in the diffusion-controlled regime defines an upper bound and approaches the exact result at large diffusion coefficients. In the present paper, we derive the applicability criteria of the WF approximation by a memory function expansion combined with scaling arguments, and establish its relation to chain length, contact radius, and quenching rate. Within the region of validity for the WF approximation, we investigate the chain length dependence of the fluorescence lifetime measurement of a single Gaussian chain.

Although the relaxation of each normal mode of a polymer chain is Gaussian and Markovian, the end-to-end distance motion is generally non-Markovian. The quenching rate probed by fluorescence experiments is a function of the end-to-end distance and is in general not localized. If the quenching rate is infinitely fast and localized at the contact radius, the fluorescence is quenched upon first contact and the fluorescence lifetime becomes the first contact time or the first passage time. Yet this equivalence does not hold for a general quenching rate. Several simplified approaches have been proposed to address the fluorescence-quenching problem in a polymer chain. The Szabo–Schulten–Schulten (SSS) theory in Ref. 12 considers the effective diffusion of the end-to-end distance. A similar approach has been adopted to study the semiflexible polymers where a potential of mean force is mapped out from the equilibrium distribution of the end-to-end distance.[20] These reduced approaches neglect the non-Markovian nature of the end-to-end distance motion and

[a)]Author to whom correspondence should be addressed. Electronic mail: jianshu@mit.edu

do not necessarily describe the complete range of scaling relations between the first passage time and the contour length even for a simple Rouse chain. The WF approximation, although derived from a Markovian approximation for the quenching rate, works surprisingly well for a Gaussian chain and has been validated in a set of experiments and simulations.[2] For a diffusion process with a delta-function reaction rate, the quenching rate degree of freedom is Markovian and the WF approximation becomes exact. In Appendix A, we demonstrate this special case and the equivalence of the delta-function sink and the radiative boundary condition. In general, the applicability of WF approximation to a polymer system depends strongly on the contour length, the experimental quenching rate, the contact radius, the solvent viscosity, etc. In Sec. II, we discuss a generalized expansion of the WF approximation and a quantitative criteria for its reliability for a Gaussian chain.

For real polymers such as polypeptide chains, fluorescence lifetime measurements provide a quantitative tool to investigate the effects of chain contour length and stiffness. In a series of fluorescence quenching experiments, Eaton *et al*. studied these effects in the diffusion-controlled regime by varying intervening residues on a polypeptide chain. In their experiments, a fluorophore-quencher pair, for example, tryptophan and cysteine, are attached to the ends of a polypeptide chain. On optical excitation, the fluorophore is excited to a state with long lifetime, and is quenched efficiently upon contact with the quencher. The average quenching lifetime $\langle t \rangle$ clearly indicates the loop formation. Their experiments show that the effective quenching rate $k_{\text{eff}} = 1/\langle t \rangle$ exhibits an $N^{-3/2}$ dependence for long chains and has a nonmonotonic N dependence for short chains due to chain stiffness. In Sec. III C, a theoretical calculation is carried out to investigate this observation. Fluorescence resonance energy transfer (FRET) is another promising tool to probe polymer dynamics on short time and length scales. In FRET experiments donor and acceptor dye molecules are attached at two different points of one polymer or two different polymers. Upon excitation, nonradiative energy transfer from donor to acceptor may occur. The energy transfer rate has an inverse power-law dependence on the donor–acceptor distance. According to Förster theory, $K(R) = k_F (R/R_F)^{-6}$, with R_F the Förster radius at 50% transfer efficiency. A recent Brownian dynamics simulation by Srinivas and Bagchi showed a power-law dependence of the average lifetime on the chain length with an exponent of 2.6.[21] A power-law dependence with a smaller exponent was observed earlier by Pastor, Zwanzig, and Szabo in a simulation of the first passage time in a Rouse chain.[13] The larger exponent observed in the FRET simulation may arise from the $1/R^6$ dependence, or an enhancement of the effective persistence length from the excluded volume effects. In Sec. III we analyze the contour length dependence based on the semiflexible Gaussian chain model for polymers.[22]

II. MEASUREMENTS AND CALCULATIONS OF AVERAGE FLUORESCENCE LIFETIME

Let us consider a general scenario where a fluorophore is attached to one end of a chain polymer and a quencher is attached to the other end. The fluorescence-quenching process determined by the rate K is coupled to the internal relaxation of the polymer described by the relaxation operation $\mathcal{L}$. The survival probability of the fluorescence evolves as

$$\dot{P}(t) = \mathcal{L}P(t) - KP(t), \tag{1}$$

where the operator $\mathcal{L}$ represents the internal relaxation of the polymer and reduces to the Smoluchowski operator for simple diffusion, and $K = K(R)$ is the first-order reaction rate coefficient which depends on the fluorophore-quencher distance R. In bulk measurements, we optically excite the fluorophores attached to polymers in solution to their excited states at zero time and then monitor the total fluorescence intensity. The average fluorescence lifetime is obtained by integrating the decay profile of fluorescence intensity. In single-molecule experiments, short laser pulses are constantly applied to the single polymer at high frequency so that the fluorophore is quickly pumped back to its excited state once the fluorescence is quenched by the quencher. As a result, fluorescence trajectories are registered with instantaneous interruptions of quenching events. With these sequences of events, we can determine the fluorescence lifetime distribution function and other single-molecule quantities, such as the multiple-event density and high order memory functions discussed later in this section. In comparison to bulk measurements, these single-molecule trajectories provide detailed information of the polymer dynamics without inhomogeneous averages, which is a powerful tool to probe conformational dynamics on the molecular level.

A. First passage time and fluorescence lifetime

When the quenching process is localized, e.g., $K(R) = q_0 \delta(R-a)$, the fluorescence-quenching event is a clear indication of the formation of a physical contact. For $q_0 \to \infty$, the fluorescence is quenched upon first contact and the quenching reaction reduces to the Smoluchowski boundary condition. In this limit the quenching time or the fluorescence lifetime becomes the first passage time or the first contact time. In reality, the fluorescence is not quenched completely upon contact. As a result, the fluorescence lifetime includes contributions from the second contact, the third contact, and so forth. These additional contributions distinguish the fluorescence lifetime from the first passage time.

In Fig. 1, we plot the simulation results of a Rouse chain. The simulation details are elaborated in Sec. II D. The delta-function quenching rate $K(R) = q_0 \delta(R-a)$ is approximated by a narrow Gaussian and the contact radius is identical to the bond length. The mean first passage time is obtained from simulation assuming the same Smoluchowski boundary condition as in Ref. 13. At large q_0's, the average fluorescence lifetime approaches the mean first passage time. This result demonstrates the difference between the fluorescence lifetime and the first passage time, and this difference approaches zero in the limit $q_0 \to \infty$.

In Appendix A, we discuss the equivalence of radiative boundary condition and delta-function sink. For the reaction rate given by $K(r) = k_0 \delta(r-a)$ and r governed by the diffusion operator $\mathcal{L}$, the WF approximation becomes exact and $\hat{\chi}_1(0)$ is the first contact time. In the limit $k_0 \to \infty$, the aver-

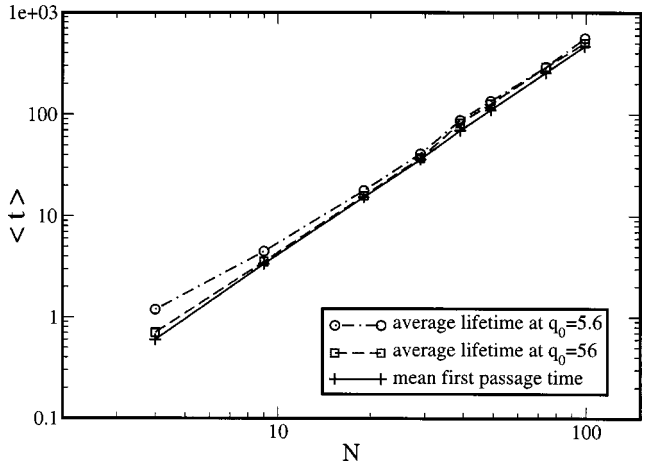

FIG. 1. The difference between the mean first passage time and the average fluorescence lifetime. The delta-function quenching rate $K(R)=q_0\delta(R-a)$ is approximated by a narrow Gaussian in the simulation. The mean first passage time is obtained by assuming a Smoluchowski boundary condition.

age fluorescence lifetime is equivalent to the first passage time. In general, this equivalence does not hold when K is not infinitely fast and localized, or when $\mathcal{L}$ is not a diffusion operator.

B. Generalized Wilemski–Fixman expansion and single-molecule measurements

In the time domain, the quenching time distribution is the time derivative of the survival probability $F(t)=-dS(t)/dt$, which in Laplace space is

$$\hat{F}(z)=1-z\hat{S}(z). \tag{2}$$

For the diffusion-controlled reaction, the survival probability is $\hat{S}(z)=\langle(z+K-\mathcal{L})^{-1}\rangle$, where $\langle\cdots\rangle$ represents the ensemble average over the initial equilibrium configuration. As such, the mean quenching time $\langle t\rangle=-\hat{F}'(z=0)$ is equivalent to the average lifetime $\hat{S}(0)$. We can also demonstrate this relation within the modulated reaction model discussed in literature.[22–24] The probability density for a quenching event at time t is the cumulative probability to have the previous quenching event occurring at least t time before, giving

$$F(t)=\left\langle \int_t^\infty Ke^{-(K-\mathcal{L})\tau}Kd\tau\right\rangle. \tag{3}$$

The Laplace transform of the quenching time distribution is $\hat{F}(z)=z^{-1}\langle K[(K-\mathcal{L})^{-1}-(z+K-\mathcal{L})^{-1}]K\rangle$, which is equivalent to Eq. (2). This interpretation relates the quenching time distribution function to the single event distribution function, $\langle Ke^{-(K-\mathcal{L})\tau}K\rangle$, discussed in Refs. 23 and 24, which provides a unique way to determine the lifetime distribution function in single-molecule measurements.

To calculate the average fluorescence lifetime, we derive a rigorous expression of $\hat{S}(0)$. First we expand the survival probability as

$$\begin{aligned}\hat{S}(z)&=\left\langle\frac{1}{z+K-\mathcal{L}}\right\rangle\\&=\frac{1}{z}-\frac{1}{z^2}\langle K\rangle+\frac{1}{z^2}\langle K\hat{G}(z)K\rangle\\&\quad-\frac{1}{z^2}\langle K\hat{G}(z)K\hat{G}(z)K\rangle+\cdots\\&=\frac{1}{z}-\frac{1}{z^2}\langle K\rangle+\frac{1}{z^2}\left(\frac{\langle K\rangle^2}{z}+\langle K\hat{G}'K\rangle\right)\\&\quad-\frac{1}{z^2}\left(\frac{\langle K\rangle^3}{z^2}+2\langle K\hat{G}'K\rangle\frac{\langle K\rangle}{z}+\langle K\hat{G}'K\hat{G}'K\rangle\right)+\cdots,\end{aligned} \tag{4}$$

where $\hat{G}(z)=1/(z-\mathcal{L})$ is the Laplace transform of the Green's function $G(t)$ for internal relaxation, and $\hat{G}'(z)=\hat{G}(z)-P_{\rm eq}/z$ is obtained by subtracting the asymptotic limit $P_{\rm eq}/z$ from $\hat{G}(z)$. This expansion is identical to Eq. (10) in paper I of this series,[19] and is cited here for completeness. Then we re-sum the expansion, leading to

$$\hat{S}(z)=\frac{1+\Omega(z)}{k+z[1+\Omega(z)]}. \tag{5}$$

$k=\langle K\rangle$ is the homogeneous average of the reaction rate and $\Omega(z)=k^{-1}\Sigma_{n=0}^{\infty}(-1)^n\hat{Y}_n(z)$. Given the definition of the nth order memory function $\hat{\chi}_n(z)=k^{-(n+1)}\langle K\hat{G}'K\cdots\hat{G}'K\rangle$, we obtain the relation between $\hat{Y}_n(z)$ and the memory functions

$$\begin{aligned}&k^{-2}\hat{Y}_0(z)=\hat{\chi}_1(z),\\&k^{-3}\hat{Y}_1(z)=\hat{\chi}_2(z)-\hat{\chi}_1^2(z),\\&k^{-4}\hat{Y}_2(z)=\hat{\chi}_3(z)-2\hat{\chi}_1(z)\hat{\chi}_2(z)+\hat{\chi}_1^3(z),\\&k^{-(n+1)}\hat{Y}_{n-1}(z)=\hat{\chi}_n(z)-\sum_{j=1}^{n-1}\hat{\chi}_j(z)k^{-(n-j+1)}\hat{Y}_{n-j-1}(z).\end{aligned} \tag{6}$$

The re-summation result for the special case with $\mathcal{L}$ being the diffusion operator is derived in Ref. 19. Under the Markovian assumption of the quenching rate, $\hat{\chi}_n(z)=\hat{\chi}_1^n(z)$, we have $Y_{n\geqslant 1}=0$, and the expansion in Eq. (5) reduces to the well-known WF approximation

$$\hat{S}(z)=\frac{1+k\hat{\chi}_1(z)}{k+z[1+k\hat{\chi}_1(z)]}. \tag{7}$$

In fact, the nth order memory function can be measured directly from single-molecule experiments. In these experiments, a high frequency laser source is constantly applied so that the fluorophore is re-excited once the fluorescence is quenched. Consequently, temporal trajectories of quenching events in a single polymer are recorded. The $n+1$ event density $\hat{N}_{n+1}=k^{-1}\langle K\hat{G}(z)K\cdots K\hat{G}(z)K\rangle$ can be collected from these single-molecule trajectories and provides a comprehensive probe of the nth order memory function[23,24]

$$\hat{\chi}_n(z)=k^{-n}\left[\hat{N}_{n+1}(z)-z^{-1}\sum_{j=0}^{n-1}k^{j+1}\hat{\chi}_j(z)\hat{N}_{n-j}(z)\right] \tag{8}$$

with $\hat{N}_1=1$ and $\hat{\chi}_0(z)=1$. Equations (5) and (8) provide a link between the ensemble-averaged fluorescence intensity measurements and the single-molecule multi-event measurements.

C. Criteria for applying WF approximation

The average fluorescence lifetime is obtained easily from the expansion

$$\langle t\rangle=\hat{S}(0)=k^{-1}+k^{-2}\sum_{n=0}^{\infty}(-1)^n\hat{Y}_n(0), \tag{9}$$

which reduces to the WF approximation $\langle t\rangle=1/\langle K\rangle+\hat{\chi}_1(0)$ if truncated at the first order. The accuracy of the WF approximation is determined by the contribution from higher order terms in the expansion. Although a rigorous proof of the convergence criteria for the alternating series expansion is not available, we can estimate the higher order contributions for a Gaussian chain. From previous discussion, we know that all the nonzero contributions of the higher order terms arise from the non-Markovian nature of the quenching rate. Rescaling the time by the slowest relaxation time τ_R, we estimate $\hat{Y}_n(0)\propto k^{n+2}\tau_R^{n+1}$, which leads to the sufficient criteria for the applicability of the WF expression

$$k\tau_R<1. \tag{10}$$

This criteria involves two time scales of the reaction dynamics: the homogeneous average reaction time $1/k$ and the slowest relaxation time τ_R. Equation (10) requires the relaxation time scale to be smaller than the reaction time scale, which is consistent with the local equilibrium approximation.[13,25]

For a quenching reaction with a delta-function sink $K(R)=q_0\delta(R-a)$ on a Rouse chain, the homogeneous average rate is $k\sim q_0a^2/N^{3/2}b^3$, given that the contact radius a is normally much smaller than the equilibrium end-to-end distance. The slowest relaxation time is $\tau_R\sim N^2b^2/D_0$ where b is the equilibrium bond length. Combination of k and τ_R yields an explicit expression of the criteria in Eq. (10)

$$k\tau_R\sim q_0b\frac{N^{1/2}b^2}{D}\left(\frac{a}{b}\right)^2. \tag{11}$$

Therefore, for a Gaussian chain of fixed bond length the WF approximation is accurate for short contour length N, small contact radius a, small quenching rate q_0, or large diffusion coefficient D_0.

D. Simulation of a Rouse chain

To examine the accuracy of the criteria in Sec. II C, we perform computer simulations to compute the average fluorescence lifetime in a Rouse chain. In our simulation, we consider a Rouse chain with a fluorophore attached to one end and a quencher attached to the other end. The potential energy of the chain is

$$\beta U=\frac{3}{2b^2}\sum_{n=1}^{N-1}(\mathbf{r}_n-\mathbf{r}_{n+1})^2, \tag{12}$$

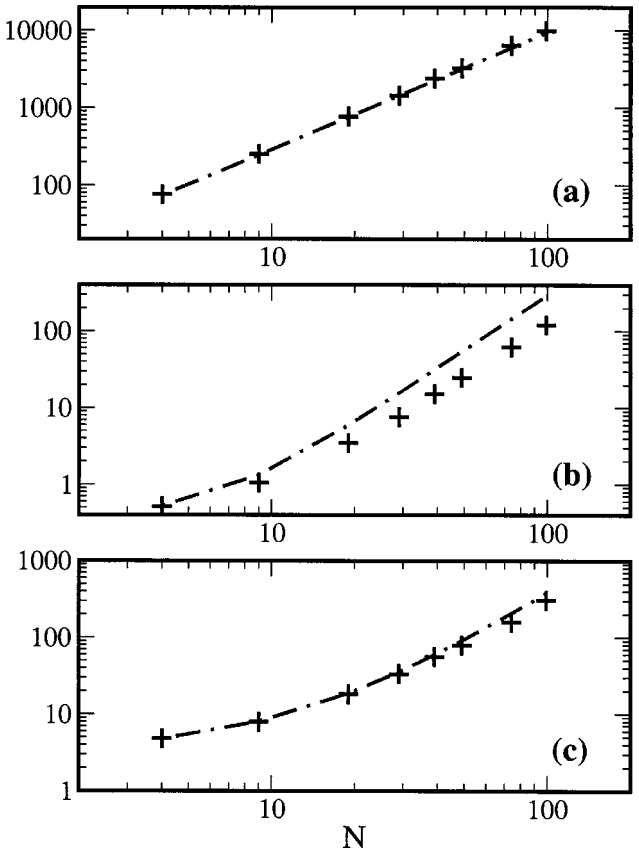

FIG. 2. The average fluorescence lifetime from the WF approximation compared to the simulation: (a) $a=0.1$, $q_0=5.6$; (b) $a=1.0$, $q_0=5.6$; (a) $a=1.0$, $q_0=0.56$. The simulation results are shown as plus symbols and the WF approximation $\langle t\rangle=1/\langle K\rangle+\hat{\chi}_1(0)$ is shown as dot-dashed lines. As a, q_0, or N decreases, the WF approximation approaches the simulation results.

where b is the equilibrium bond length and $\mathbf{r}_n$ is the position of the nth bead. The quenching time is averaged over many trajectories. For each trajectory, the initial configuration is generated from the equilibrium distribution $P_{\mathrm{eq}}=\mathcal{N}\exp[-\beta U]$, and $\mathcal{N}$ is the normalization factor. Here we adopt the Ermak–McCammon algorithm to generate dynamic trajectories of Rouse chain.[13,26] The evolution of the nth bead's position is

$$\mathbf{r}_n(t+\Delta)=\mathbf{r}_n(t)-D_0\nabla_n\beta U\Delta+\mathbf{x}_n, \tag{13}$$

where Δ is the time step and $\mathbf{x}_n$ is a random displacement from a normal distribution with zero mean and variance $2D_0\Delta$. The quenching probability for each time step is $1-\exp[-K(R)\Delta]$ and R is the end-to-end distance at time t. Upon detection of a quenching event in our simulation, we record the quenching time and restart the simulation with a new initial configuration. In our simulation we take $b=1$, $D_0=1$ and use a specific functional form of quenching rate,[3,4] $K(R)=q_0\exp[-\gamma(R-a)]$ with $\gamma=a^{-1}$.

The results for the average fluorescence lifetime are displayed in Fig. 2. The criteria in Eq. (11), although obtained from simple scaling arguments, is surprisingly reliable. At $a=0.1$, $q_0=5.6$, the WF expression reproduces all the simulation results for the contour lengths up to $N=100$. At a larger contact radius $a=1$ with q_0 fixed, the WF approxima-

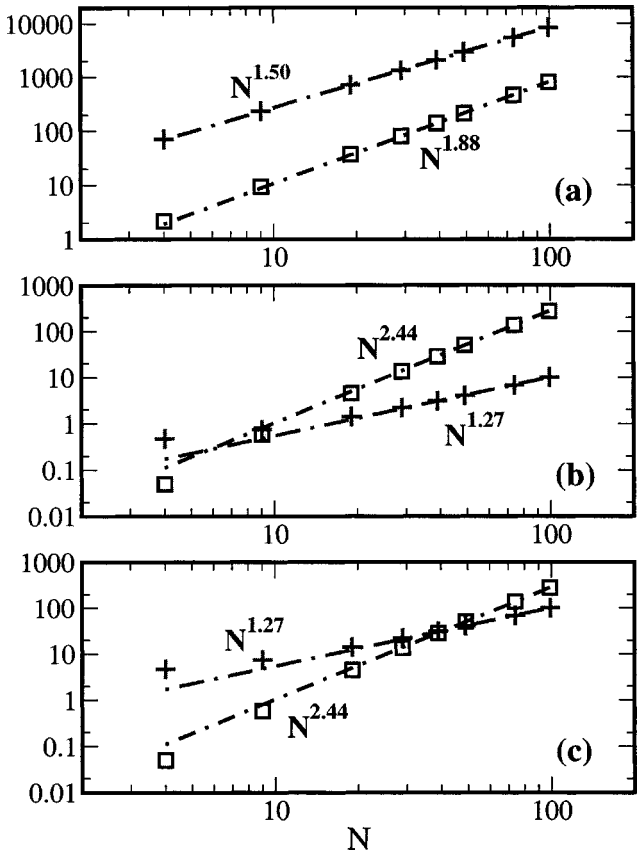

FIG. 3. Scaling of $1/\langle K\rangle$ and $\hat{\chi}_1(0)$: (a) $a=0.1$, $q_0=5.6$; (b) $a=1.0$, $q_0=5.6$; (a) $a=1.0$, $q_0=0.56$. $1/\langle K\rangle$ is shown as plus symbols and $\hat{\chi}_1(0)$ is shown as square symbols. The scaling relations are shown in dot-dashed lines.

tion deviates from the simulation result, and the deviation becomes more prominent at larger contour lengths. At lower quenching rates q_0, the WF approximation shows excellent agreement with simulation. In all three subplots, the agreements are generally better for shorter Rouse chains. As predicted by Eq. (11), for short contour lengths, small contact radii or small q_0, the relaxation time scale is much smaller than the reaction time scale. In this limit, the Markovian assumption of the quenching rate or the local equilibrium approximation becomes valid, so the WF approximation is accurate.

It can be seen from Fig. 2 that the WF results have different slopes in the log–log plot at different contact radii. As demonstrated in Sec. II C, the WF approximation includes two contributions, the homogeneous average rate $1/\langle K\rangle$ and the average relaxation time $\hat{\chi}_1(0)$. To examine the details of the length dependences, we plot these two contributions separately in Fig. 3. The scalings of both quantities with contour length show strong dependencies on the contact radius; $1/\langle K\rangle$ scales as $N^{3/2}$ at $a=0.1$ and has a smaller scaling exponent at a larger contact radius $a=1$. The scaling exponent of $\hat{\chi}_1(0)$ decreases with the contact radius. Different contour length dependences are also observed for different contact radii with Smoluchowski boundary conditions, as shown by Pastor and Szabo's simulations, which corresponds to a delta-function sink in the limit $q_0\to\infty$ (see Sec. II). Based on our calculation and their simulation, different scaling relations for different radii arise naturally from $\hat{\chi}_1(0)$. We investigate the contour length dependence in the following section and discuss Fig. 3 further.

III. CONTOUR LENGTH DEPENDENCE AND SEMIFLEXIBILITY

For synthetic and biological polymers, fluorescence lifetime measurements provide a quantitative tool to investigate the dependence of fluorescence lifetime on contour length. Real polymers have excluded volume, hydrodynamic, and monomer-specific interactions, resulting in variations in chain stiffness over a wide range of length scales. In this section we study the effects of semiflexibility and contour length dependence on conformational dynamics of single macromolecules. We limit our discussion to fluorescence quenching and fluorescence resonance energy transfer (FRET). The major difference between them is the distance dependence of $K(R)$: the fluorescence-quenching rate falls off exponentially, $K(R)=q_0\exp[-\gamma(R-a)]$, and the FRET rate has an inverse power-law dependence, $K(R)=k_F(R/R_F)^{-6}$.

For a Gaussian chain, the equilibrium distribution of the end-to-end distance is

$$P_{\mathrm{eq}}(R)=4\pi R^2[2\pi\langle R^2\rangle/3]^{-3/2}\exp[-3R^2/2\langle R^2\rangle], \quad (14)$$

where $\langle R^2\rangle$ is the mean square end-to-end distance. The Green's function of the end-to-end distance is

$$G(R,t|R_0)=\sqrt{\frac{2}{\pi}}\frac{\sqrt{3}R}{\sqrt{\langle R^2\rangle}R_0\phi(t)\sqrt{1-\phi^2(t)}}\times\exp\left[-\frac{3(R^2+\phi^2(t)R_0^2)}{2\langle R^2\rangle[1-\phi^2(t)]}\right]\times\sinh\left(\frac{3RR_0\phi(t)}{\langle R^2\rangle[1-\phi^2(t)]}\right), \quad (15)$$

where $\phi(t)$ is the normalized distance correlation function defined in the literature.[22] For a Rouse chain, the explicit form of $\phi(t)$ is given by Szabo and others.[13,25]

In paper I,[19] we demonstrate that either the reaction or the relaxation time scale can dominate chain conformational kinetics depending on the experimental scenarios. The present discussion centers on the diffusion-controlled regime, which has been measured experimentally and studied numerically.[2,4,13] The WF theory defines two fundamental quantities, the homogeneous average rate $k=\langle K\rangle$ and the memory function $\chi_1(t)$. Both are sensitive to the functional form of the reaction rate. In Secs. III A and III B, we assume a delta-function reaction sink $K(R)=q_0\delta(R-a)$ and analyze the dependence of k and $\hat{\chi}_1(0)$ on the persistence length and chain length. Here, a is the contact radius for fluorescence quenching processes and the Förster radius R_F for FRET processes. In Sec. III C, we use an exponential quenching rate and compare our predictions with the fluorescence-quenching experiment by Eaton and his coworkers. In Sec. III D, we discuss the lifetime and yield measurements in FRET experiments.

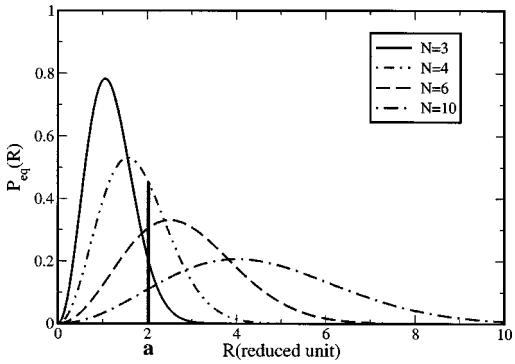

FIG. 4. Equilibrium distribution of the end-to-end distance for the semiflexible Gaussian chain with the persistence length $L_p=2$. The length unit is the equilibrium bond length b. The delta-function sink is represented as a solid bar at $R=a$. The N dependence of the homogeneous average rate k is illustrated by the crossing points of the delta-function sink and the equilibrium distributions.

A. Homogeneous average rate k

Given the equilibrium distribution in Eq. (14) and the delta-function sink, we have

$$k \propto \frac{a^2}{\langle R^2\rangle^{3/2}} \exp\left[-\frac{3a^2}{2\langle R^2\rangle}\right], \tag{16}$$

where the mean square end-to-end distance $\langle R^2\rangle$ is a function of N. As illustrated in Fig. 4, at extremely small N, $a^2 > \langle R^2\rangle$, the homogeneous average rate k is a probe of the right edge of the distribution and is dominated by the exponential factor $\exp[-3a^2/2\langle R^2\rangle]$. For a^2 smaller than $\langle R^2\rangle$, the probe falls on the left edge of the distribution and k has a complicated dependence on N for small N. In the limit of large N, and the homogeneous average rate k is dominated by the prefactor $a^2/\langle R^2\rangle^{3/2}$. The scaling exponents of k with contour length in this regime, $a^2 \ll \langle R^2\rangle$, is summarized in Table I: For a flexible chain with persistence length $L_p \ll N$, the mean square end-to-end distance is $\langle R^2\rangle = 2Nb^2L_p$ and k scales as $N^{-3/2}$; while for a stiff chain with persistence length $L_p \gg N$, $\langle R^2\rangle = N^2b^2$ and k scales as N^{-3}.

B. Memory function $\hat{\chi}_1(0)$

The memory function $\chi_1(t)$ for a delta-function sink is rigorously obtained as

$$\chi_1(t) = \frac{\langle KG(t)K\rangle}{k^2} - 1$$
$$= \frac{1}{2x_0\phi(t)\sqrt{1-\phi^2(t)}} \sinh\left(\frac{2x_0\phi(t)}{1-\phi^2(t)}\right) \times \exp\left[-\frac{2x_0\phi^2(t)}{1-\phi^2(t)}\right] - 1, \tag{17}$$

where $x_0 = 3a^2/2\langle R^2\rangle$ and $\phi(t)$ is the normalized distance correlation function. To estimate the contour length dependence, we expand $\chi_1(t)$ at small $2x_0\phi(t)/[1-\phi^2(t)]$, giving

$$\chi_1(t) \approx [1-\phi^2(t)]^{-3/2} - 1 - 2x_0\phi^2(t)[1-\phi^2(t)]^{-5/2} + \cdots. \tag{18}$$

At short times, both ends move independently, giving $\phi(t) \approx 1 - 6D_0/\langle R^2\rangle t$.[22] In this time region, $\phi(t)$ is close to 1 and the expansion is no longer valid. We can estimate the invalid region of the expansion as $2x_0\phi(t)/[1-\phi^2] > 1$, giving $\phi(t) > 1 - x_0$ or equivalently $t < \langle R^2\rangle x_0/6D_0 = a^2/4D_0$. Accordingly, we break the full integration into two parts $\hat{\chi}_1(0) = I_1 + I_2$ with

$$I_1 = \int_0^T \chi_1(t)dt, \quad \text{and } I_2 = \int_T^\infty \chi_1(t)dt, \tag{19}$$

where $T = a^2/4D_0$. Within $[0,T]$, $\chi_1(t) \approx 1/4\sqrt{2}x_0^{3/2}$, yielding an estimation of the first term

$$I_1 \sim T/4\sqrt{2}x_0^{3/2} = \langle R^2\rangle^{3/2}/24\sqrt{3}D_0a. \tag{20}$$

Compared to the first passage time $\sqrt{2\pi}N^{3/2}b^3/12\sqrt{2}D_0a$ in the SSS theory where only the diffusion of the end-to-end distance is considered,[13] I_1 is off by a factor of $2\sqrt{2\pi}$. The second term I_2 is essentially dominated by the slowest relaxation time τ_R, yielding a different scaling

$$I_2 \sim \tau_R. \tag{21}$$

It is clear that two competing processes contribute differently to $\hat{\chi}_1(0)$. The diffusive motion of end-to-end vector dominates at short time, while the collective relaxation of the polymer dominates at long time. The relative weights of these two contributions are determined by the contact radius a. $\hat{\chi}_1(0)$ is dominated by I_1 at small a and by I_2 at large a, and the crossover falls roughly into the region where these two integrals are comparable. The length dependence of $\hat{\chi}(0)$ is determined by both I_1 and I_2. For the dependence on semiflexibility and contact radius, we make several observations.

(1) For a flexible chain when $L_p \ll N$, the mean square end-to-end distance is $\langle R^2\rangle = 2Nb^2L_p$ and the slowest relaxation time is $\tau_R \sim N^2L_pb^2/D_0$. Hence, $I_1 \sim N^{3/2}$ dominates at small a while $I_2 \sim N^2$ dominates at large a, and the crossover occurs around $b/a \sim \sqrt{N}$. Our numerical calculation of $\hat{\chi}_1(0)$ for a Rouse chain ($L_p = 1/2$) with a delta-function sink corroborates this result. As shown in Fig. 5, $\hat{\chi}_1(0)$ scales as $N^{2.08}$ for $a=1$, $N^{1.68}$ for $a=0.1$, and $N^{1.53}$ for $a=0.01$, respectively. The calculation strongly confirms the two competing contributions and that $I_1 \sim N^{3/2}$ dominates over I_2

TABLE I. Summary of the scaling exponents of $1/k$ and $\hat{\chi}_1(0)$ with the contour length in the large N limit where $a^2 \ll \langle R^2\rangle$. Depending on the persistence length L_p, this regime is separated into two regions corresponding to $L_p \ll N$ and $L_p \gg N$, respectively. Small a represents the limit $b/a \gg \sqrt{N}$ while large a represents the opposite limit. HI refers to hydrodynamic interactions incorporated in the Zimm model.

		$\hat{\chi}_1(0)$ without HI		$\hat{\chi}_1(0)$ with HI	
	$1/k$	Small a	Large a	Small a	Large a
Flexible chain $L_p \ll N$	3/2	3/2	2	3/2	3/2
Stiff chain $L_p \gg N$	3	3	4	3	7/2

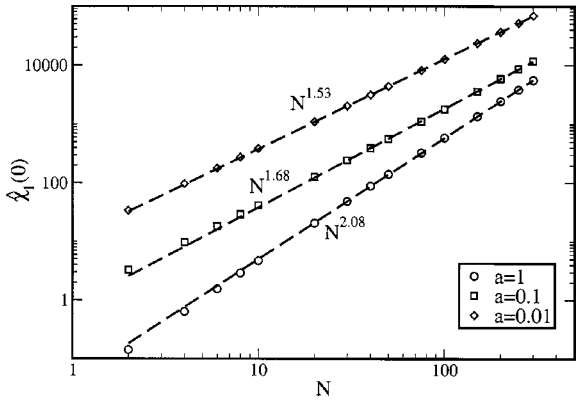

FIG. 5. The contour length dependence of $\hat{\chi}_1(0)=\int_0^\infty \chi_1(t)dt$ for a delta-function sink. $\hat{\chi}_1(0)$ scales as $N^{2.08}$ at $a=1$, $N^{1.68}$ at $a=0.1$, and $N^{1.53}$ at $a=0.01$. Exact calculations are plotted with symbols and the scaling relations are shown in dashed lines.

$\sim N^2$ as the contact radius decreases. The decreasing scaling exponents with the contact radii are also observed for an exponential quenching rate in Fig. 3, where $\hat{\chi}_1(0)$ scales as $N^{2.44}$ at $a=1.0$ and $N^{1.88}$ at $a=0.1$. Although the contour lengths are not large enough to show the asymptotic scalings, we are still able to distinguish the leading contributions at different radii, which is a generic effect of the two competing processes.

(2) For a stiff chain when $L_p \geqslant N$, the mean square end-to-end distance is $\langle R^2\rangle = N^2b^2$ and the slowest relaxation time is $\tau_R \sim N^4b^2/L_pD_0$. Consequently, I_1 scales with the contour length as N^3 and I_2 scales as N^4. Srinivas and Bagchi's simulations[21] for a semiflexible chain with L_p comparable to the contour length and excluded volume effects reported an exponent of 2.6. This result lies between the flexible chain limit and the stiff chain limit.

(3) In the presence of hydrodynamic interactions, the normal modes of a semiflexible chain are approximated using the pre-averaged approximation for the hydrodynamics tensors introduced by Zimm.[27,28] Details can be found in our previous work.[22] The scaling relations are summarized as:

$$\begin{cases} \text{When } L_p \ll N, & I_1 \sim N^{3/2}, \quad I_2 \sim N^{3/2}; \\ \text{When } L_p \gg N, & I_1 \sim N^3, \quad I_2 \sim N^{7/2}. \end{cases} \tag{22}$$

Consequently, $\hat{\chi}_1(0)$ scale with N and has a smaller exponent in presence of hydrodynamic effects.

In short summary, both $1/k$ and $\hat{\chi}_1(0)$ scale with the contour length for long polymer chains. The scaling exponents are listed in Table I. At small contact radius, $\hat{\chi}_1(0)$ is dominated by the integral I_1, which depends only on the equilibrium end-to-end distance. I_1 has the same scaling exponents with and without hydrodynamic interactions. While at large contact radius, $\hat{\chi}_1(0)$ is dominated by the integral I_2, which depends on the slowest relaxation time and has different scaling exponents with and without hydrodynamic interactions.

C. Intramolecular fluorescence quenching: Comparison with Eaton's experiments

Quenching of the long-lived triplet state of tryptophan by cysteine provides an accurate way to measure the rate of loop formation in polymer chains. With tryptophan at one end of a semiflexible peptide and cysteine at the other, Eaton *et al.* were able to obtain the diffusion-limited rate of contact formation. They measured the length dependence and the viscosity dependence of the effective quenching rate by varying the number of intervening Ala-Gly-Gln sequences. The effective quenching rate is defined as the inverse of average lifetime, $k_{\text{eff}}=1/\langle t\rangle \approx k/[1+k\hat{\chi}_1(0)]$. In this section, we mainly address two important experimental findings by the Eaton group.

(1) The scaling of the effective quenching rate approaches $N^{-3/2}$ for chain length $N\sim 15$ but depends less on N for shorter peptides.[2]
(2) The diffusion coefficient required to fit the diffusion-influenced rate is about ten times smaller than the value expected for free diffusion of the contacting residues.[4]

From the Gaussian distribution in Eq. (14) and the exponential quenching rate $K(R)=q_0\exp[-\gamma(R-a)]$, the homogeneous average quenching rate is obtained as

$$\begin{aligned} k=\langle K\rangle &= \int_a^\infty q_0 e^{\gamma(R-a)} P_{\text{eq}}(R)dR \\ &= \frac{1}{\sqrt{2\pi\zeta}}\exp\left[-\frac{1}{2\zeta}\right]\left(2-2\zeta+\sqrt{2\pi\zeta}(1+\zeta)\right. \\ &\quad \left.\times\exp\left[\frac{(1+\zeta)^2}{2\zeta}\right]\operatorname{erfc}\left[\frac{1+\zeta}{\sqrt{2\zeta}}\right]\right) \end{aligned} \tag{23}$$

with $\zeta=\gamma^2\langle R^2\rangle/3$. Given that $\langle R^2\rangle = 2NL_pb^2$ for a flexible chain and $\gamma=a^{-1}$, ζ is a large number for small a and large N. In the asymptotic limit $\zeta\to\infty$, $\langle K\rangle$ reduces to $q_0\sqrt{8/\pi}\zeta^{-3/2}$ and scales as $N^{-3/2}$. For the case where the contact radius is about the bond length, the asymptotic scaling is approached for large contour lengths. Furthermore, $1/\langle K\rangle$ does not exhibit a monotonic dependence on the contour length for short polypeptide chains due to the chain stiffness.

In Fig. 6, the effective quenching rate is calculated numerically with and without hydrodynamic interactions. The contour length dependence of the effective quenching rate is close to the experimental observation.[2] For short peptide chains, $k\hat{\chi}_1(0)\ll 1$, the overall quenching rate is dominated by the k given in Eq. (23). At large N, the probe radius a falls on the left edge of the equilibrium distribution and k decreases with increasing N, which agrees favorably with the calculations of Eaton *et al.*[4] Our calculations predict a weaker dependence on N around $N=3$ due to the chain stiffness. The probe position a for a short peptide chain with $N=3$ occurs at the right edge of the distribution, as illustrated in Fig. 4, and produces the small decline of the curve. In our simulation, the effective quenching rate for long peptide chains is dominated by $1/\hat{\chi}_1(0)$. In the absence of hydrodynamic interactions, $1/\hat{\chi}_1(0)$ scales with the contour length as N^{-2} where the contact radius is comparable to the bond

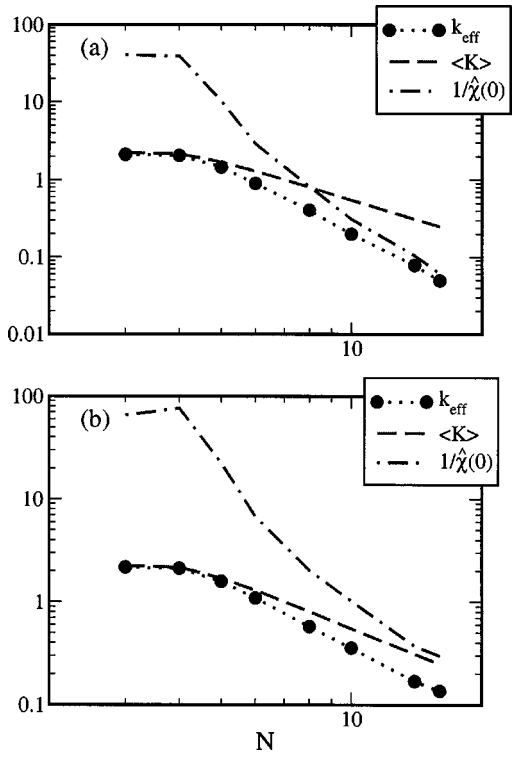

FIG. 6. Dependence of the effective quenching rate $k_{\text{eff}}=1/\langle t\rangle$ on the chain length (a) without hydrodynamic interactions and (b) with hydrodynamic interactions. The time unit is $b^2/6D_0$. The persistence length is $L_p=2$, and the quenching rate at contact is estimated from experimental data to be $q_0=5.6$. Due to the chain stiffness, k_{eff} does not have a monotonic scaling for very short chains. For a relatively long chain, the effective rate is dominated by $1/\hat{\chi}_1(0)$, yielding N^{-2} scaling without hydrodynamic interactions and $N^{-3/2}$ scaling with hydrodynamic interactions, respectively. The $N^{-3/2}$ scaling was observed by Eaton *et al.*[2,4] for $N\sim 15$.

length. While in the presence of hydrodynamic interactions, $1/\hat{\chi}_1(0)$ scales with the contour length as $N^{-3/2}$, which was also observed by Eaton *et al.* for $N\sim 15$.

To better approximate the exponential quenching rate with the delta-function sink, the effective probe radius should be greater than the contact radius a. Real polymers are closer to the worm-like chain model than the semiflexible Gaussian chain model. The semiflexible Gaussian chain model normally gives smooth equilibrium distribution $P_{\text{eq}}(R)$, as shown in Fig. 4, while the worm-like chain model predicts much sharper decay at right edges of the distribution.[4,29] Therefore, the worm-like chain model predicts sharper decay of k as a falls at the right edge of the distribution. As a combination of these two effects, the homogeneous average quenching rate $k=\langle K(R)\rangle$ should decline faster at small contour lengths, as demonstrated in Eaton's experiments.[4]

In general, the effective diffusion process of the end-to-end distance R is non-Markovian. A natural way to introduce an effective diffusion coefficient is

$$D_{\text{eff}}=\frac{\langle R^2\rangle}{6\int_0^\infty \phi(t)dt}. \tag{24}$$

This definition differs from $D_0=2k_BT/\zeta$ used in Pastor, Zwanzig and Szabo's work[13] and reflects the independent motion of the polymer beads at both ends while containing no information on the collective motion of the whole polymer chain. A simple calculation shows that D_{eff} given by Eq. (24) is about seven times smaller than $2k_BT/\zeta$ for chains of length $N=10$ at 1 cp and 293 K, in agreement with the experimental findings of Eaton *et al.*[2,4]

D. Fluorescence resonance energy transfer: Lifetime and quantum yield

Another laser-induced fluorescence spectroscopy technique that provides complementary information on the internal relaxation of biopolymers is fluorescence resonance energy transfer (FRET). This technique has been extensively used in single-molecule studies of conformational dynamics of proteins, DNAs, RNAs and other biomolecules.[7–9] The inverse power-law transfer rate diverges at $R\to 0$ where the transition dipole–dipole interaction no longer holds. To facilitate the calculation, we use a modified expression for $K(R)$

$$K(R)=\frac{k_F}{\epsilon+(R/R_F)^6}, \tag{25}$$

where ϵ is a small quantity that represents the breakdown of the weak dipole–dipole interaction for small R. This expression reduces to the quantum yield for FRET processes when $\epsilon=1$. Thus the discussion applies to quantum yield measurements as well. The Fourier transform of the FRET rate is

$$K(\mathbf{q})=\frac{2\pi^2 k_F R_F^2}{3q\epsilon^{2/3}}\left\{\exp[-qR_F\epsilon^{1/6}]+\exp\left[-\frac{qR_F\epsilon^{1/6}}{2}\right]\cdot\left[-\cos\left(\frac{\sqrt{3}}{2}qR_F\epsilon^{1/6}\right)+\sqrt{3}\sin\left(\frac{\sqrt{3}}{2}qR_F\epsilon^{1/6}\right)\right]\right\}, \tag{26}$$

which reduces to $2\pi^2R_F^3k_F/3\sqrt{\epsilon}$ when $qR_F\epsilon^{1/6}\ll 1$. Considering that ϵ is a small number, the FRET rate is well approximated by a delta-function sink $K(R)=k_0\delta(R-R_F)$ with $k_0=\pi R_Fk_F/(6\sqrt{\epsilon})$.[22] The contour length dependence roughly follows Table I.

IV. CONCLUSION AND DISCUSSIONS

Here we summarize our findings. For the fluorescence-quenching process in a polymer chain, the fluorescence lifetime is not equivalent to the first passage time unless the quenching rate is infinitely fast and localized at the contact radius. Based on a generalized Wilemski–Fixman formalism, the fluorescence lifetime distribution function can be decomposed into memory functions that are measurable in single-molecule experiments. A sufficient criteria, $k\tau_R<1$, for the validity of the WF approximation is obtained from the expansion for a Gaussian process. This criteria for a Gaussian chain predicts that $\langle t\rangle=1/k+\hat{\chi}_1(0)$ is a reliable approximation for small contact radii, slow quenching rates or short contour lengths. The theoretical prediction is corroborated by computer simulations of quenching processes in a Rouse chain.

The dependence of physical properties, such as average fluorescence lifetime, on the chain length is crucial for characterizing polymers and can be used to quantitatively determine the chain stiffness. For reaction kinetics in the diffusion-controlled regime, the average fluorescence lifetime is well approximated by $\langle t\rangle = 1/k + \hat{\chi}_1(0)$. For localized reaction rate $K(R) = q_0\delta(R-a)$, where a is the contact radius for fluorescence quenching or the Förster radius for FRET, $1/k$ scales as $N^{3/2}$ for flexible chains and N^3 for stiff chains. The scaling of the $\hat{\chi}_1(0)$ with the contour length N is characterized by two competing processes, the independent motion of the end-to-end vector and the slowest relaxation of polymer. The former dominates at a small contact radius and the latter dominates at a large contact radius. For flexible chains, $\hat{\chi}_1(0)$ scales as N^2 at a large contact radius and $N^{3/2}$ at a small contact radius, while for stiff chains, $\hat{\chi}_1(0)$ scales as N^3 at a large contact radius and N^4 at a small contact radius. The scaling relation for a flexible chain agrees well with Szabo's simulation.[13] Srinivas and Bagchi's simulations of a semiflexible chain with L_p comparable to contour length gives an exponent of 2.6 for $\langle t\rangle$, which lies between the flexible and the stiff limits.[21] In the presence of hydrodynamic interactions, $\hat{\chi}_1(0)$ has a smaller scaling exponent, which scales as $N^{3/2}$ for a flexible chain, and as N^3 at a small contact radius and $N^{7/2}$ at a large contact radius for a stiff chain.

An application of the scaling relations to the fluorescence-quenching experiments by Eaton and his group clarifies two findings:

(1) For intramolecular fluorescence-quenching processes, the effective quenching rate is given by $k_{\text{eff}} = 1/\langle t\rangle$. For long polymer chains, the effective quenching rate is dominated by $\hat{\chi}_1(0)$ and exhibits $N^{-3/2}$ scaling. For short polymer chains, the effective quenching rate is determined by k, the homogeneous average rate; k decreases as N increases when the contact radius falls on the left edge of the equilibrium distribution $P_{\text{eq}}(R)$, and increases with N when the contact radius falls on the right edge of the equilibrium distribution. Our calculations agree quantitatively with the experimental data of Eaton *et al.*[4] where the effective quenching rate k_{eff} approaches the $N^{-3/2}$ scaling for long polymer chains and depends less on N for short chains.

(2) Through normal mode decomposition, non-Markovian relaxation of the end-to-end distance for a semiflexible chain is composed of a number of Markovian processes. The end-to-end distance undergoes an effective diffusion on the potential of mean force. Phenomenologically, the effective diffusion coefficient is related to the distance correlation function by $6D_{\text{eff}}\int_0^\infty \phi(t)dt = \langle R^2\rangle$. Numerical calculations demonstrate that D_{eff} for $N=10$ is about seven times smaller than the bead diffusion coefficient $D_0 = 2k_BT/\zeta$ at 1 cp and 293 K. This theoretical prediction agrees with recent experimental findings by Eaton and his co-workers. The effective diffusion constant required to fit the diffusion-influenced rates in their experiments is about ten times smaller compared to the free diffusion of the residues.[2,4]

ACKNOWLEDGMENTS

This research was supported by the NSF Career Award (Grant No. Che-0093210) and the Petroleum Research Fund administrated by the American Chemical Society. J.C. is a recipient of the Camille Dreyfus Teacher-Scholar Award. We would like to thank Dr. Eaton for sending us their preprint.

APPENDIX A: EQUIVALENCE OF BOUNDARY CONDITION AND DELTA-FUNCTION SINK

For a one-dimensional delta-function sink, $K(x) = k_0\delta(x-a)$, the homogeneous average rate is $k = k_0 P_{\text{eq}}(a)$. Let us now obtain $\hat{\chi}_1(0)$ from the rate–rate correlation function

$$k^2\hat{\chi}_1(0) = \int \eta(x)P_{\text{eq}}(x)(K(x)-k)dx. \tag{A1}$$

With the adjoint operator $\mathcal{L}^+$ definition which was used by Szabo–Schulten–Schulten in their solution to diffusion with an absorbing boundary, $\eta(x)$ satisfies

$$\mathcal{L}^+\eta(x) = -(K(x)-k). \tag{A2}$$

The adjoint operator $\mathcal{L}^+ = e^{\beta U}\partial_x(D(x)e^{-\beta U}\partial_x)$ depends on the general position dependent diffusion coefficient $D(x)$. Considering now the boundary conditions $\eta(x\to\pm\infty)=0$, we have

$$\eta(x) = \int_{-\infty}^{x}\frac{e^{\beta U(y)}}{D(y)}dy\int_y^\infty (K(\xi)-k)e^{-\beta U(\xi)}d\xi. \tag{A3}$$

Substituting this equation into Eq. (A1) and averaging over the equilibrium distribution $P_{\text{eq}}(x) = (\int_{-\infty}^{\infty}e^{-\beta U(y)}dy)^{-1}e^{-\beta U(x)}$, we obtain

$$k^2\hat{\chi}_1(0) = \left(\int_{-\infty}^{\infty}e^{-\beta U(y)}dy\right)^{-1}\int_{-\infty}^{\infty}\frac{e^{\beta U(x)}}{D(x)} \times dx\left[\int_x^\infty e^{-\beta U(y)}(K(y)-k)dy\right]^2. \tag{A4}$$

Therefore, $\hat{\chi}_1(0)$ is given by

$$\hat{\chi}_1(0) = \left(\int_{-\infty}^{\infty}e^{-\beta U(y)}dy\right)^{-1}\int_{-\infty}^{a}\frac{e^{\beta U(x)}}{D(x)} \times dx\left[\int_{-\infty}^{x}e^{-\beta U(y)}dy\right]^2 + \left(\int_{-\infty}^{\infty}e^{-\beta U(y)}dy\right)^{-1} \times \int_a^\infty\frac{e^{\beta U(x)}}{D(x)}dx\left[\int_x^\infty e^{-\beta U(y)}dy\right]^2. \tag{A5}$$

And the average lifetime is

$$\langle t\rangle = \frac{1}{k} + \left(\int_{-\infty}^{\infty}e^{-\beta U(y)}dy\right)^{-1}\int_{-\infty}^{a}\frac{e^{\beta U(x)}}{D(x)} \times dx\left[\int_{-\infty}^{x}e^{-\beta U(y)}dy\right]^2 + \left(\int_{-\infty}^{\infty}e^{-\beta U(y)}dy\right)^{-1} \times \int_a^\infty\frac{e^{\beta U(x)}}{D(x)}dx\left[\int_x^\infty e^{-\beta U(y)}dy\right]^2. \tag{A6}$$

Equation (A6) is exactly a sum of contributions from the left and the right regions of the boundary with proper weight. It is the same result as the SSS theory with radiation boundary conditions. It proves the equivalence of delta-function sink and radiation boundary conditions. In the limit $k_0 \to \infty$, the radiative boundary becomes the absorbing or Smoluchowski boundary and the fluorescence lifetime becomes $\hat{\chi}_1(0)$ in Eq. (A5). This is the same as the first passage time given by the Szabo–Schulten–Schulten theory.[12]

In higher dimensions, the real reactive sink is defined as a hyper plane in a multi-dimensional space. For example, $K(r)=k_0\delta(r-a)$ is actually a reactive spherical surface in a three-dimensional space. Under such conditions, the whole space can be separated into two regions, inside and outside the reactive surface. This separation scheme given in Eq. (A6) still holds for such cases. With a reactive surface, the Wilemski–Fixman approximation is only exact when the reaction coordinate r is Markovian, for example, $\mathcal{L}=D\nabla\cdot[\nabla+\nabla\beta U(r)]$. For this special case, we can prove that the reaction rate degree of freedom $k(r)$ is precisely Markovian. Hence the average lifetime is

$$\langle t\rangle = \frac{1}{k} + \frac{1}{D}\left[\int_0^\infty r^2 e^{\beta U(r)} dr\right]^{-1} \cdot \left\{ \int_0^a e^{\beta U(r)} r^{-2} dr \left[\int_0^r e^{-\beta U(\rho)} \rho^2 d\rho\right]^2 + \int_a^\infty e^{\beta U(r)} r^{-2} dr \left[\int_r^\infty e^{-\beta U(\rho)} \rho^2 d\rho\right]^2 \right\}. \quad \text{(A7)}$$

For non-Markovian reaction coordinate, the reaction rate degree of freedom is not Markovian even when the reaction rate is localized. Therefore the Wilemski–Fixman approximation is no longer exact.

[1] O. Bieri, J. Wirz, B. Hellrung, M. Schutkowski, M. Drewello, and T. Kiefhaber, Proc. Natl. Acad. Sci. U.S.A. **96**, 9597 (1999).
[2] L. J. Lapidus, W. A. Eaton, and J. Hofrichter, Proc. Natl. Acad. Sci. U.S.A. **97**, 7220 (2000).
[3] L. J. Lapidus, W. A. Eaton, and J. Hofrichter, Phys. Rev. Lett. **87**, 258101 (2001).
[4] L. J. Lapidus, P. J. Steinbach, W. A. Eaton, A. Szabo, and J. Hofrichter, J. Phys. Chem. B **106**, 11628 (2002).
[5] T. Basche, W. E. Moerner, M. Orrit, and U. P. Wild, *Single Molecule Optical Detection, Imaging and Spectroscopy* (VCH, Wein Heim, 1997).
[6] X. S. Xie and J. K. Trautman, Annu. Rev. Phys. Chem. **49**, 441 (1998).
[7] A. A. Deniz, T. A. Laurence, G. S. Beligere, M. Dahan, A. B. Martin, D. S. Chemla, P. E. Dawson, P. G. Schultz, and S. Weiss, Proc. Natl. Acad. Sci. U.S.A. **97**, 5179 (2000).
[8] D. S. Talaga, W. L. Lau, H. Roder, J. Tang, Y. Jia, W. F. DeGrado, and R. M. Hochstrasser, Proc. Natl. Acad. Sci. U.S.A. **97**, 13021 (2000).
[9] X. Zhuang, H. Kim, M. J. B. Pereira, H. P. Babcock, N. G. Walter, and S. Chu, Science **296**, 1473 (2002).
[10] G. Wilemski and M. Fixman, J. Chem. Phys. **60**, 866 (1974).
[11] G. Wilemski and M. Fixman, J. Chem. Phys. **60**, 878 (1974).
[12] A. Szabo, K. Schulten, and Z. Schulten, J. Chem. Phys. **72**, 4350 (1980).
[13] R. W. Pastor, R. Zwanzig, and A. Szabo, J. Chem. Phys. **105**, 3878 (1996).
[14] N. Agmon and J. J. Hopfield, J. Chem. Phys. **78**, 6947 (1983).
[15] G. H. Weiss, J. Chem. Phys. **80**, 2880 (1984).
[16] R. Zwanzig, Acc. Chem. Res. **23**, 148 (1990).
[17] R. Zwanzig, J. Chem. Phys. **97**, 3587 (1992).
[18] J. Wang and P. G. Wolynes, Chem. Phys. Lett. **212**, 427 (1993).
[19] S. Yang and J. Cao, J. Chem. Phys. **121**, 562 (2004), preceding paper.
[20] S. Jun, J. Bechhoefer, and B.-Y. Ha, Europhys. Lett. **64**, 420 (2003).
[21] G. Srinivas and B. Bagchi, J. Phys. Chem. B **105**, 9370 (2001).
[22] S. Yang, J. B. Witkoskie, and J. Cao, J. Chem. Phys. **117**, 11010 (2002).
[23] J. Cao, Chem. Phys. Lett. **327**, 38 (2000).
[24] S. Yang and J. Cao, J. Phys. Chem. B **105**, 6536 (2001).
[25] J. Sung and S. Lee, J. Chem. Phys. **105**, 9050 (2001).
[26] D. L. Ermak and J. A. McCammon, J. Chem. Phys. **69**, 1352 (1978).
[27] B. H. Zimm, J. Chem. Phys. **24**, 269 (1956).
[28] M. Doi and S. F. Edwards, *The Theory of Polymer Dynamics* (Oxford University Press, New York, 1986).
[29] Z. Wang and D. E. Makarov, J. Chem. Phys. **117**, 4591 (2002).